4D seismic pressure-saturation inversion at Gullfaks field, Norway

David Lumley, Don Adams, Mark Meadows, Steve Cole and Ray Ergas* of 4th Wave Imaging, a Californian company specializing in advanced 4D seismic software development, describe its application of proprietary pressure-saturation inversion to the Statoil operated Gullfaks field, offshore Norway.

Time-lapse 4D seismic reservoir monitoring is experiencing rapid acceptance as a practical reservoir management tool, as evidenced by three full days of technical presentations on the topic at the recent June 2003 EAGE Conference in Stavanger, Norway. The 4D seismic technique is useful to help map bypassed oil, monitor costly injection programs, and improve our understanding of reservoir compartmentalization and the fluid-flow properties of faults.

Most of the applications to date have tended to be qualitative rather than quantitative. For example, 4D seismic practitioners often examine time-lapse seismic amplitude maps and develop a qualitative interpretation of where they think fluids are flowing in the reservoir, constrained by supporting data such as geologic control, well logs and engineering production information. However, there is a growing desire to obtain more quantitative results from 4D seismic data, for example, the ability to create pressure and saturation maps or volumes with calibrated physical units of saturation and pressure to assist engineering workflows and reservoir management decisions.

This paper presents a case study in which we apply quantitative Pressure-Saturation Inversion (PSI) technology developed by 4th Wave Imaging to the 4D seismic project at the Gullfaks field, offshore Norway.

Gullfaks field

The Gullfaks field is operated by Statoil and is located in Block 34/10 in the Norwegian North Sea along the western margin of the North Viking Graben. The main producing reservoirs are variable thickness Jurassic sands up to 300 m thick in the Brent, Cook and Statfjord formations. Gullfaks is produced with vertical and deviated water injectors and producers, in addition to some more recent horizontal production wells. Further information on the Gullfaks field can be found in publications by Stronen & Digranes (2000), Landro (2001), and Alsos et al. (2002), for example.

Figure 1 shows a map of the Gullfaks field mapped at the Top Brent marker. The study area for this article is indicated by the shaded yellow region. Green lines represent well paths emanating from the three platforms. Red outlined regions represent areas where repeat 4D seismic streamer data could not be acquired due to the proximity of the platforms and other surface obstacles, causing data 'holes' with varying mute depths in the final seismic image volumes.

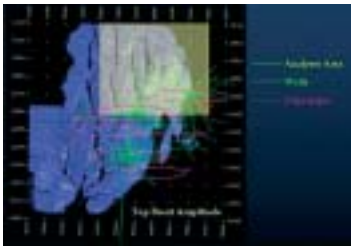

Figure 1 *Map of Gullfaks reservoir, top Brent. The yellow shaded region is the study area, green lines are well paths, and the red outlines holes in seismic data coverage.*

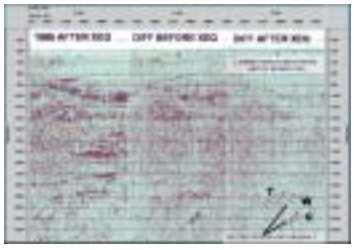

Figure 2A *4D seismic before and after XEQ processing. Left – 1985 seismic baseline data; centre – contractor difference cube before XEQ; and right – improved difference cube after XEQ processing with ProMAX4D software. Note that the shallow false anomalies caused by event ghosting due to misalignment have been largely suppressed after XEQ processing.*

In this project we focused on the Tarbert reservoir at the top of the Brent group, and the Cook reservoir at depth below it. The study area was selected by Statoil since there have been some anomalous production results in this area,

**www.4thwaveimaging.com*

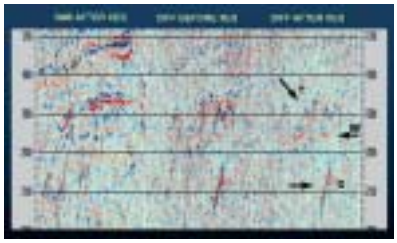

Figure 2B *Same as Figure 2A but zoomed in on the reservoir region. Note that the false ghosting anomalies at the top Tarbert (T) reservoir and base BCU have been suppressed, revealing a clear pattern of fault-block-constrained reservoir anomalies, and a much clearer image of the oil-water contact (W). The Cook reservoir anomaly (C) has also been improved.*

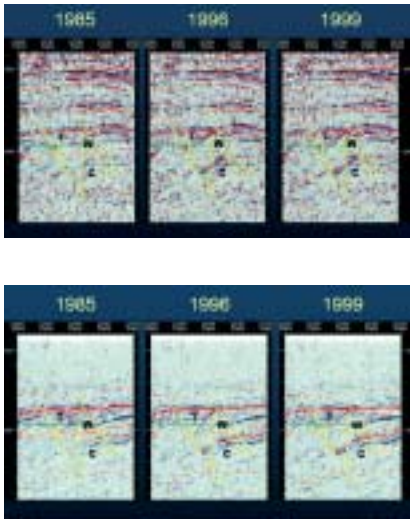

Figures 3A, 3B *Time-lapse AVO seismic sections after 4D AVO balancing. 3A is the near offset section, 3B is the far offset section. Note that the time-lapse AVO anomalies on the Tarbert (T) event and the Cook (C) event are quite different, since the Tarbert is saturation-dominated and the Cook is pressure-dominated. [Instructions – please position Figure 3A immediately above 3B]*

and mixed success at prior attempts to estimate both pressure and saturation effects from the 4D seismic data. The Cook reservoir in this area was also of interest because of large pressure effects potentially overwhelming any saturation effects.

4D Seismic XEQ processing

We received three vintages of seismic streamer data from Statoil including surveys from 1985, 1996 and 1999. The data sets consisted of three final migration offset cubes (near, mid, far) per survey, including multiple passes of match filtering and global corrections applied by the processing contractor. In order to apply our pressure-saturation inversion technology, we first had to ensure that the 4D seismic data sets met the highest standards of repeatability required by time-lapse AVO analysis.

We applied our 4D seismic Cross-Equalization (XEQ) processing flow and found that, although the contractor had done a reasonably good job at processing the cubes, it was possible to significantly improve the repeatability and ultimately the quality of the pressure-saturation inversion results. The XEQ processing flow draws from our 4D seismic prestack and poststack processing toolbox, available commercially as ProMAX4D from Landmark, and was customized for the Gullfaks 4D seismic data sets to consist of constrained time and space variant: data masking, gain compensation, frequency spectra balancing, differential statics, differential waveform phase, seismic event alignment, and final optimized scaling and differencing.

Figure 2A shows a full section view of the baseline data and the difference data before and after XEQ. Note that the shallow section of the contractor difference data (before XEQ) is much noisier than after XEQ, containing false 'ghosting' anomalies caused by misalignment of strong non-reservoir reflections. Figure 2B shows a zoom of the reservoir region. Note that the contractor difference section before XEQ shows falsely strong anomalies along the top Brent markers at about 1870 ms, partially due to real reservoir changes and partially due to strong ghosting of the Base Cretaceous Unconformity (BCU) reflector. In contrast, results after XEQ processing show a much cleaner difference section above and below the producing reservoirs, real difference anomalies correlating to production data in the Tarbert reservoir (T) in block-by-block structures along the BCU, a much enhanced image of the Brent oil-water contact (W) in each fault block, and a crisper image of the seismic anomaly related to production activity in the deeper Cook reservoir (C).

For time-lapse AVO purposes, a 4D AVO balancing was performed using a combination of the ProMAX4D toolbox and 4th Wave Imaging proprietary in-house software, by applying AVO amplitude and spectral corrections to a matrix of all nine seismic cubes: three vintages by three offsets. Figure 3A shows the near offset sections after 4D AVO balancing for all three survey vintages, and Figure 3B shows the same for the far offset sections. Note the different time-lapse AVO behaviour of the Tarbert reservoir (T) compared to the Cook reservoir (C), which will later be shown to be related to saturation-dominated effects in the Tarbert versus pressure-dominated effects in the Cook.

Pressure-saturation inversion

As a developer of pressure-saturation inversion technology for 4D seismic applications (see Cole et al., 2002; 2003; and Lumley et al., 2003), 4th Wave Imaging has recently made the technology available with the release of the PSI interactive software package so that geoscientists and engineers can invert time-lapse seismic data sets to produce quantitative estimates of reservoir pressure and saturation changes, including uncertainty analysis. In this section we discuss the application of PSI to the Gullfaks 4D seismic project.

After the 4D seismic data has been pre-conditioned, as described in the previous section, but before PSI can be run, we need to extract and calibrate 4D seismic attributes, perform a reservoir rock and fluid physics analysis, and interactively optimize the inversion parameter set. Horizon surfaces were re-picked with high resolution to isolate the Tarbert and Cook reservoir zones for time-lapse AVO analysis. Several attribute extractions were performed in SeisWorks and analyzed for correlation with production engineering information; the 'Average Reflection Strength' attribute was selected as optimal for this study. These attribute maps were further calibrated with 4D seismic modelling tools at selected wells with know pressure and saturation changes, and in isolated non-producing blocks. Figure 4 shows an example of the high repeatability we were able to obtain at the Tarbert level, even though the two surveys shown are spaced 14 years apart. These attribute maps were subsequently prestack-inverted to produce Shuey slope-intercept maps, and P- and S-impedance maps.

We performed a rock and fluid physics analysis using core measurement data and PVT data supplied by Statoil. We determined regression parameters for dry modulus (Kdry) and dry shear bulk modulus (Gdry) as a function of porosity, clay content and pressure (Figure 5). This analysis predicted that for an anticipated reservoir pressure change of 25 bars, Kdry would change by about 2-3%, and Gdry would change by about 5-7%. We later found by post-inversion PSI uncertainty analysis that the shear modulus effects predicted from core data are probably at least three times stronger (more sensitive) to pressure change than the real response of the in-situ reservoir rocks, indicating that the cores were probably damaged (perhaps micro-fractured) along the way from the reservoir to the lab, resulting in an anomalous high core-data pressure sensitivity.

With this information in hand, we used the rock physics modeling tools and 4D data analysis within PSI to interactively optimize the pressure-saturation inversion parameters. Figure 6 shows the pressure and saturation axis determination for the Tarbert reservoir in the attribute crossplot domain of PSI required for the inversion. A final step in the PSI inversion uses engineering production data to calibrate the pressure and saturation results. For the saturation calibration we used time-lapse saturation logs provided by Statoil (Figure 7), converted them to TVD, and averaged the saturation changes in depth with a seismic spatial wavelet to get the 'true' change in saturation that the seismic waves would have been able to 'see'. We interpolated these with calendar time, since logs are rarely collected at the same time as

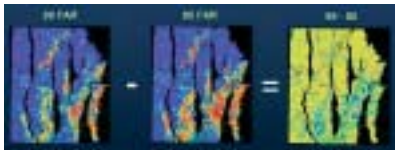

Figure 4 *Time-lapse far offset attribute maps at the Tarbert reservoir after 4D AVO balancing and attribute analysis.*

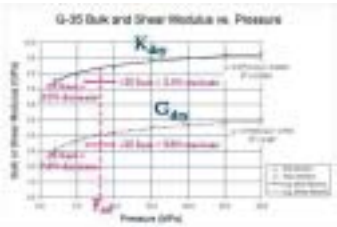

Figure 5 *Core data analysis for a Tarbert core sample. Regressions for dry bulk (Kdry) and shear (Gdry) moduli as a function of pressure. Pdiff is the differential (overburden minus pore) pressure of the reservoir.*

Figure 6 *PSI inversion axis determination by rock physics modelling analysis. The interactive software allows the user to model the effect on seismic attributes of various changes in pressure(Pp), saturation (Sw), and rock and fluid properties.*

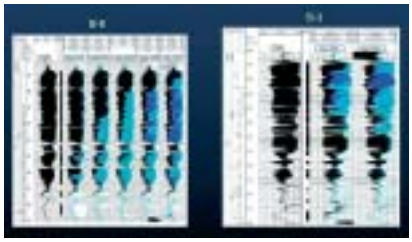

Figure 7 *Time-lapse saturation logs in the Tarbert reservoir at the B-3 and B-8 wells, converted to TVD. Note that the B-8 well is being swept from the base upwards, whereas the B-3 well is being swept from the top downwards.*

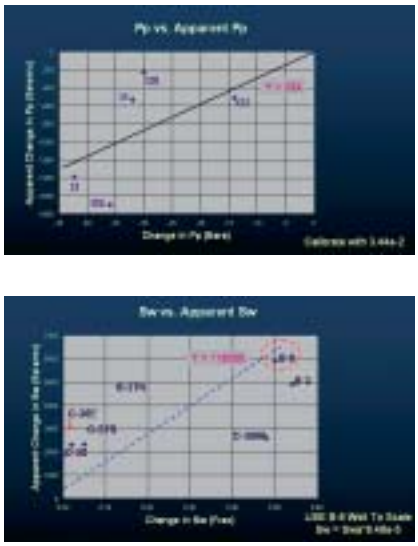

Figure 8A, 8B *Calibration crossplots for water saturation (8A) and pressure (8B). 'True' changes in saturation and pressure are averaged over a seismic spatial wavelength, and crossplotted against the seismic-derived PSI estimate extracted near the well location. Pressure data are averaged over each producing fault block. [Instructions – please position Figure 8A side-by-side and to the left of Figure 8B]*

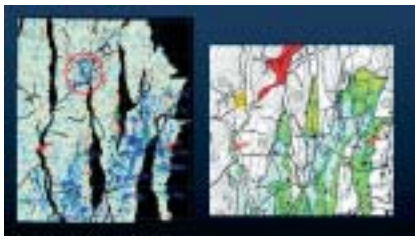

Figure 9 *Tarbert PSI saturation-change map (left) compared to recent Statoil drainage map (right). The PSI map represents the change in water saturation from 1985 (pre-production) to 1999. Dark blue is a saturation change of up to 0.8 saturation units, white represents zero saturation change.*

the seismic surveys. For the pressure calibration, we obtained bottom-hole pressure data from Statoil at various wells, averaged on a block-by-block basis. Then we crossplotted the 'apparent' change in saturation and pressure obtained from our PSI estimates extracted at well locations, against the 'true' change in saturation and pressure as described above (Figures 8A and 8B). We fit polynomial functions to these crossplotted calibration data, including uncertainty error bars in both dimensions, and weighting factors that depend on the reliability of each true saturation or pressure data point (for example, how close in time was the log measurement to the seismic survey?).

Figures 9 and 10 show the results of pressure-saturation inversion for the Tarbert reservoir obtained in the manner described above. The Tarbert saturation-change map shows excellent correlation with Statoil's recent engineering drainage map, whereas the Tarbert pressure-change map shows reasonable pressure changes local to producing and injecting wells, but is dominated overall by large-scale noise. Figures 11 and 12 show striking pressure- and saturation-change probability maps for the Cook reservoir. These were also obtained using PSI technology, but using Shuey slope-intercept attributes and a 'probability-of-change' hypothesis-testing algorithm instead of the attribute crossplot inversion method described for the Tarbert work flow. The Tarbert and Cook results will be discussed further in the interpretation section of this paper.

Uncertainty analysis

In delivering quantitative pressure and saturation results, it is useful to perform an accompanying uncertainty analysis. If we estimate that the pressure has changed by, for example, 35 bars at a particular location, we would also like to specify the error in that estimate. The usefulness of the pressure-saturation estimate depends on whether the error is smaller or larger than the estimate value itself (e.g., 35 bars plus or minus 5 bars or 500 bars?).

We have developed a full set of linearized and fully non-linear Monte Carlo uncertainty analysis tools to address this issue. We can probe the sensitivity of the PSI pressure-saturation results as a function of any single inversion parameter (oil GOR for example), or subset of parameters (e.g., GOR, porosity, Kdry), or all of the inversion parameters simultaneously. We can also explore the post-inversion spatial uncertainty in pressure and saturation results by performing thousands of physically-constrained realizations of the input seismic data and rock physics parameters, and then running thousands of PSI inversions to gather up the full post-inversion uncertainty statistics.

Figures 13A and 13B show the standard deviation maps in pressure and saturation obtained by this uncertainty analysis technique, which accompany the pressure and saturation estimate maps of Figures 9 and 10. Note that the standard deviation (error) in saturation in the produced areas is about 0.2 saturation units compared to saturation-change estimates on the order of 0.2-0.8 units, whereas the pressure errors are about 150 bars compared to an anticipated signal of about 20-40 bars maximum. These results inform us that the saturation estimates in most areas are well-determined, whereas the pressure estimates are largely contaminated by noise, as will be discussed in the next section.

Having generated a full *a posteriori* probability distribu-

tion function at each reservoir location, we can make virtually any statistical measure of uncertainty that we desire. Figure 14 shows one such example where we have created a map showing the probability that water saturation has increased more than 0.7 saturation units between the 1985 and 1999 4D seismic surveys. The strong blue areas in the centre of Figure 14 show a strong probability, greater than 0.6 on a scale of 0-1, that waterflood in the H fault block of the Tarbert has exceeded 0.7 saturation units, for example.

Interpretation of PSI results

Let us now make some brief interpretations of the quantitative pressure-saturation results obtained for the Tarbert and Cook reservoirs.

Figure 9 shows the Tarbert saturation-change map obtained from PSI, and a comparison to a recent Statoil engineering drainage map created from production information at wells and Statoil internal 4D seismic interpretation methods. The strongest blue colour in the PSI map is about 0.8 saturation-change units, and white is zero change. Figure 13A shows that the standard deviation error in saturation change is about 0.2 saturation units in the swept areas, so that saturation-change anomalies in Figure 9 are evidently well above the inversion noise level.

Overall there is excellent agreement between the PSI and drainage maps. However, there are important differences in detail. The left-most red arrow in Figure 9 indicates an area where Statoil was uncertain whether oil had been produced (stippled green). Our PSI saturation map shows no saturation change in this area, indicating that the oil rim had not been produced by 1999 and probably remains as bypassed oil today. Note that the saturation changes terminate abruptly at a fault just south of the red arrow, supporting our hypothesis that the fault is sealed such that no oil to the north was produced. The right-most red arrow shows a producing well that has watered out and is coloured blue in the Statoil drainage map. Our PSI saturation map is consistent in that it also shows a strong local saturation-change anomaly of about 0.7 saturation units. The area in the northern circle is an original gas cap. Water is being injected at a well here into a deeper formation (Ness), but not the Tarbert. It is apparent that the injected water may be unexpectedly penetrating the Tarbert as shown by the strong blue saturation changes in the PSI map (we have confirmed that these are not seismic wavelet sidelobe or tuning interference effects from the deeper Ness reservoir). Finally, we note a north-south anomaly in the centre of the PSI map which suggests a local pressure decrease below bubble point and gas exsolution near a horizontal producer. We have confirmed with production data that this recently drilled well is producing significantly more gas (produced GOR) than any other well in the area, but since it did not encounter free gas, it was probably drilled just below a small production-induced gas cap.

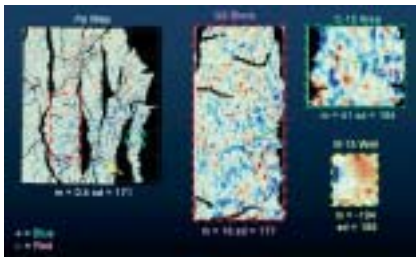

Figure 10 *Tarbert PSI pressure-change map (left) and zooms of map around interesting well locations. The red square contains the C-36 producer (centre) and the B-12 injector (south). The green square contains the C-15 producer, the yellow square contains the B-15 producer.*

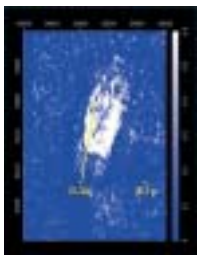

Figure 11 *Cook PSI map of 'probability that pressure has increased' on a scale of zero (blue) to 0.6 (white). Note that there is a strong pressure anomaly surrounding the B-33 horizontal injector, and east-west sealing fault compartmentalization.*

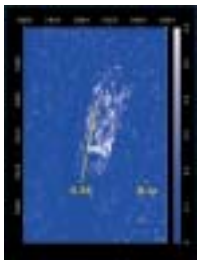

Figure 12 *Cook PSI map of "probability that water saturation has increased" on a scale of zero (blue) to 0.6 (white). Note that there is weak water saturation change in most of the compartment since B-33 injects into the water leg, but strong water saturation change to the south-east of the compartment drawn toward nearby producing well B-1.*

Figure 10 shows the Tarbert pressure-change map and some zoomed areas therein. Overall the pressure map looks very noisy. Figure 13B shows why – the uncertainty analysis has determined that the standard deviation error in pressure is on average 150 bars, which means the noise in the pressure

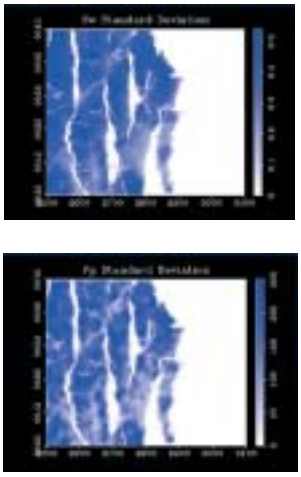

Figure 13A/13B *Standard deviation maps obtained by non-linear Monte Carlo uncertainty analysis for the Tarbert reservoir for saturation-change (13A) and pressure-change (13B). In the produced areas, the standard deviation error in water saturation is about 0.2 saturation units, and the pressure error is about 150 bars. [Instructions – please position Figure 13A side-by-side and to the left of Figure 13B]*

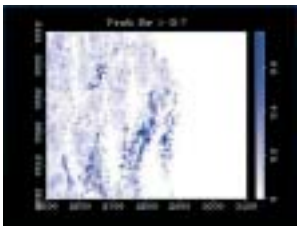

Figure 14 *Monte Carlo uncertainty analysis map showing the probability that the water saturation has increased by more than 0.7 saturation units between 1985 and 1999 in the Tarbert reservoir. Note the large probability that water has swept the central portion of the H block (dark blue) by this amount.*

estimate is about five times higher than the anticipated 30 bar signal we are looking for! We have determined that this noise is likely caused by a weak pressure signal, low sensitivity of in-situ Tarbert rocks to pressure, and seismic noise in the far offsets contaminating the seismic-derived shear information. Even though the PSI pressure map is dominated by noise, there is some evidence of real pressure signal in the Tarbert map. For example, the calibration plot of Figure 8B shows that when the PSI pressure results are averaged over each producing fault block, the PSI pressure values correlate reasonably well with the bottom-hole pressure data also averaged by block (the crossplot points would not follow a trend if the PSI results were purely noise alone). Also, in the zooms of Figure 10, the B-12 injector shows a local pressure increase in the PSI map, and the C-36 and B-15 producers show a local pressure decrease. In fact, we were informed by Statoil that the B-15 was recently sidetracked to the east and they encountered a low-pressure zone and lost the well, consistent with the local pressure decrease anomaly in the PSI map.

Figures 11 and 12 show the probability that pressure and water saturation respectively have changed in the Cook reservoir between the 1985 and 1996 seismic surveys. These maps are obtained with PSI technology but also using hypothesis-testing algorithms instead of inversion, as mentioned previously. Figure 11 shows that there is a strong probability (0.6 on a relative scale of 0-1) that pressure has increased in the Cook reservoir due to water injection in the water leg by the B-33 horizontal injection well. Also note that the east and west faults seem to be sealing and containing the pressure anomaly at this point in time, whereas the north and south ends of the compartment appear to be open. Figure 12 shows the probability that water saturation has increased around the B-33 injector, on a scale of 0-1. The main area of the compartment shows a low probability of saturation change, probably because injection is occurring in the water leg and therefore little seismic effect is visible. However, the south-east portion of the compartment shows a relatively strong probability that water saturation has increased, probably because the B-1 producing well is helping to draw injected water up-dip towards it thereby displacing produced oil.

Conclusions

We have applied our PSI pressure-saturation inversion and uncertainty analysis technology to a case study at the Gullfaks field, offshore Norway. Careful 4D seismic processing is required to perform quantitative analysis of the time-lapse data, and careful seismic attribute analysis and calibration must be performed before pressure-saturation inversion can be successfully applied. The PSI inversion work flow consists of a 4D rock and fluid physics analysis with 4D seismic attributes, and incorporation of production engineering information at a few well locations. Our results show that we can obtain striking examples of well-resolved water-swept and bypassed-oil areas in the Tarbert reservoir, but that the pressure estimates are poorly resolved due to a weak pressure signal, low sensitivity of in-situ Tarbert rocks to pressure, and seismic noise in the far offsets contaminating the seismic-derived shear information. Our results in the Cook reservoir show that a strong pressure anomaly can be estimated in the vicinity of a horizontal water injector, along with a strong water saturation anomaly drawing towards a nearby producing well, and strong evidence of east-west fault block compartmentalization at the time of the seismic surveys.

Acknowledgements

We would like to acknowledge S. Griesbach and D. Markus at 4th Wave Imaging for their significant software development contributions to the PSI pressure-saturation inversion technology featured in this paper. We would also like to thank Statoil for providing the Gullfaks 4D seismic data used in this case study, and especially L.K. Stronen, K. Duffaut, O. Eiken, T. Alsos, A-K. Furre, R. Tondel and N. Najjar (now at Aramco) for their assistance with the project.

References

Alsos, T., Eide, A.L., Hegstad, B.K., Najjar, N.F., Astratti, D., Doyen, P. and Psaila, D. (2002) From qualitative to quantitative 4D seismic analysis of the Gullfaks Field. *64th EAGE Annual Meeting*, Expanded Abstracts.

Cole, S., Lumley, D., Meadows, M., and Tura, A. (2002) Pressure and saturation inversion of 4D seismic data by rock physics forward modeling. *72nd SEG Annual International Meeting*, Expanded Abstracts, 2475-2478.

Cole, S., Lumley, D., and Meadows, M. (2003) 4D pressure and saturation inversion of Schiehallion field by rock physics modeling. *65th EAGE Annual Meeting*, Expanded Abstracts, A-05.

Landro, M. (2001) Discrimination between pressure and fluid saturation changes from time lapse seismic data. *Geophysics*, **66**, 836-844.

Lumley, D., Meadows, M., Cole, S., and Adams, D. (2003) Estimation of reservoir pressure and saturations by crossplot inversion of 4D seismic attributes. *65th EAGE Annual Meeting*, Expanded Abstracts, A-06.

Stronen, L. K. and Digranes, P. (2000) The Gullfaks field - 4D seismic enhances oil recovery and improves the reservoir description. *62nd EAGE Annual Meeting*. Expanded Abstracts.